energies

MDPI

Article

Modeling, Experimental Analysis, and Optimized Control of an Ocean Wave Energy Conversion System in the Yellow Sea near Lianyungang Port

Zhongxian Chen [1,2,*], Xu Li [1], Yingjie Cui [1] and Liwei Hong [3]

[1] School of Intelligence Manufacturing, Huanghuai University, Zhumadian 463000, China
[2] Henan Key Laboratory of Smart Lighting, Huanghuai University, Zhumadian 463000, China
[3] State Grid Langfang Electric Power Supply Company, Langfang 065000, China
* Correspondence: chenzhongxian@huanghuai.edu.cn

Abstract: In this paper, an ocean wave energy conversion system (OWECS) is modeled and experimented in the Yellow Sea near Lianyungang port, and an optimized control method based on the sliding mode control is proposed to improve the efficiency of OWECS. Firstly, a motion model of a double-buoy OWECS is presented using a complex representation method, and the analysis results indicate that the efficiency of converting ocean wave energy into the outer buoy's mechanical power is highest in a suitable ocean wave period. Secondly, a double-buoy OWECS is constructed and experimented in the Yellow Sea near Lianyungang port, which verified the correctness of the above analysis results. Lastly, in order to further improve the efficiency of the double-buoy OWECS, a sliding mode control method based on a linear generator is proposed to realize the phase synchronization between the outer buoy and ocean waves, and the simulation results may be beneficial for the next ocean test of the double-buoy OWECS.

Keywords: motion model; ocean wave energy; buoy; efficiency; optimize control

Citation: Chen, Z.; Li, X.; Cui, Y.; Hong, L. Modeling, Experimental Analysis, and Optimized Control of an Ocean Wave Energy Conversion System in the Yellow Sea near Lianyungang Port. *Energies* **2022**, *15*, 8788. https://doi.org/10.3390/en15238788

Academic Editors: Yan Bao, Guanghua He and Liang Sun

Received: 2 November 2022
Accepted: 20 November 2022
Published: 22 November 2022

1. Introduction

As a kind of renewable clean energy, ocean wave energy has attracted more and more attention in the world [1,2]. During the past 50 years, ocean wave energy conversion has been investigated and developed on a large scale, and various prototypes have been tested in the laboratory or real ocean waves [3–5]. According to the system structure, an OWECS can be classified as near-shore and offshore [6]. Regardless of the type of OWECS, buoys (or float balls) and generators are necessary.

A buoy (or float ball) is an energy transfer device that converts ocean wave energy into mechanical energy, and then drives a generator to output electrical energy. As shown in Figure 1, under the action of ocean waves, the floating ball can move in the vertical direction, which drives the linear generation to convert ocean wave energy into electrical energy. In the past 5 years, novel kinds of OWECS have been proposed and researched. For example, a hybrid OWECS which contains an oscillating water column (OWC) and oscillating buoy (OB) was proposed by Saishuai et al., and the research results indicated that the hybrid OWECS provided higher energy conversion, as well as better wave attenuation performance, compared with the isolated OWC and OB devices [7]. In addition, an oscillating buoy (OB) single-pontoon floating breakwater (SPFB) and an oscillating water column (OWC) dual-pontoon floating breakwater (DPFB) were evaluated and compared. The comparison results showed that the maximum conversion efficiency of the OWC for the optimal opening ratio was higher than that of the OB [8]. Furthermore, some other kinds of OWECS were researched in the last 5 years, such as the point-absorbing wave energy converter (WEC) with the new mechanism structure of zero pressure angle, the smart floatable open-water wave energy converter, and the variable-geometry wave energy converter [9–11].

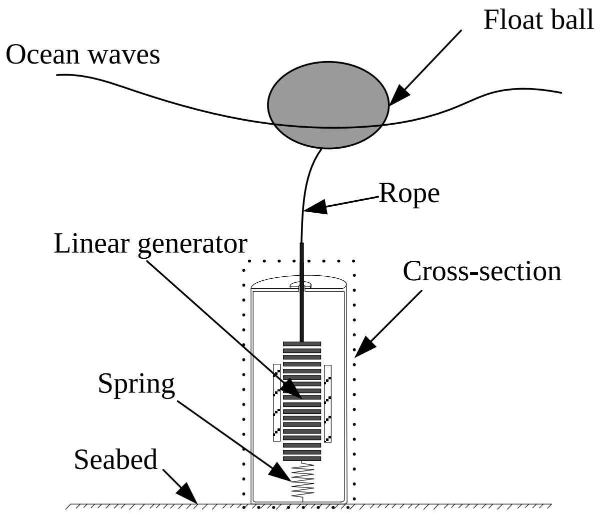

Figure 1. Structure of an ocean wave energy conversion device.

Actually, the motion of buoys (or float balls) plays an important role in the operation efficiency of an OWECS. Only when the natural frequency of buoys (or float balls) is identical to the ocean wave's frequency can the efficiency of ocean wave energy converting into electrical energy be maximized [12,13]. Therefore, the design and modeling of buoys (or float balls) is one of the important topics in the research of OWECS.

Furthermore, a generator is an energy conversion device that converts mechanical energy into electrical energy. In order to improve the operational efficiency of a generator, some novel generators have been proposed, such as the superconducting magnet-excited linear generator, linear switched reluctance generator, and Halbach magnetized linear permanent magnet generator [14–16]. Compared with conventional rotary generators, the high efficiency and simple structure make the linear generator an attractive candidate for OWECS. However, due to the variable nature of wave periods and wave heights of ocean waves, the non-controlled generator does not play a key role in the operational efficiency of OWECS [17].

In this paper, according to the wave periods of the Yellow Sea near Lianyungang port, the model test of a double-buoy OWECS was carried out in the Yellow Sea near Lianyungang port. Firstly, the motion model of a double-buoy OWECS is presented and analyzed. Secondly, a double-buoy OWECS is experimented in the Yellow Sea near Lianyungang port, proving the correctness of the analysis results of the motion model of the double-buoy OWECS. Lastly, in order to further improve the efficiency of the double-buoy OWECS, a sliding mode control method based on the linear generator is proposed and simulated in Section 4 of this paper. At the end of this paper, the principal restrictions of study in this paper are discussed.

2. Motion Model of Double-Buoy OWECS

2.1. Vertical Direction Speed of Buoy

A buoy floating in ocean waves is shown in Figure 2a. Under the action of ocean waves, the buoy can be moved in the vertical direction z, surge direction x, and sway direction y. Figure 2b shows a double-buoy OWECS with an outer buoy and inner buoy. Due to the different draught of the outer buoy and inner buoy, a relative motion between them occurs, which drives the generator (installed in the upper end of inner buoy) to convert ocean wave energy into electrical energy.

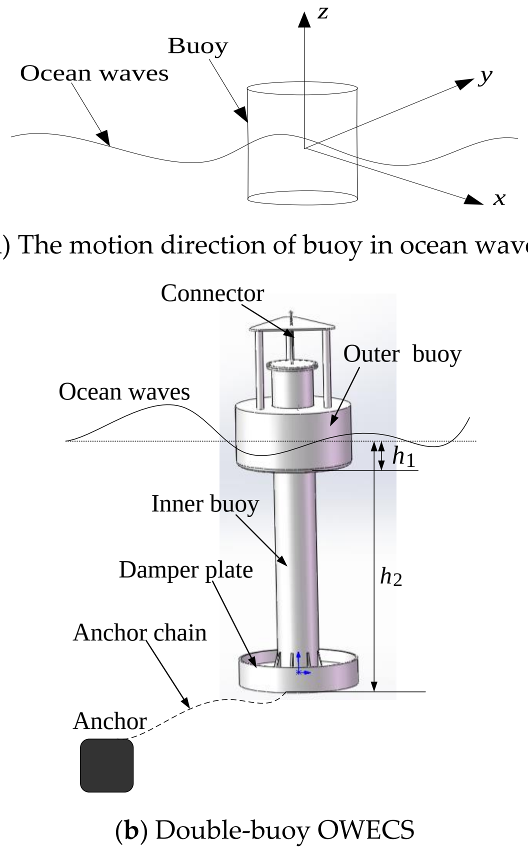

Figure 2. The operational principle of double-buoy OWECS.

In the vertical direction, the acceleration formula of buoy can be described as

$$m\hat{a}_z = \hat{F}_z + \hat{F}_r + \hat{F}_b + \hat{F}_f, \tag{1}$$

where m is the mass (in kg), $\hat{a}_z$ is the acceleration in the vertical direction, $\wedge$ represents a complex representation, $\hat{F}_z$ is the vertical direction ocean wave force, $\hat{F}_r$ is the radiation force from the relative motion between buoy and ocean waves, $\hat{F}_b$ is the hydrostatic buoyancy force, and $\hat{F}_f$ is the friction force.

Usually, the diameter of a buoy is smaller than the wavelength of ocean waves; thus, the method of Froude–Krylow force and small object approximation can be used [18]. The vertical direction ocean wave force $\hat{F}_z$ can be written as

$$\hat{F}_z = \left[\rho g S_w - \omega^2 \rho V(1+\mu_z)\right]\hat{\eta}, \tag{2}$$

where ρ is the density of ocean water, g is the acceleration due to gravity, S_w is the horizontal cross-section of buoy, ω is the angular frequency of ocean waves, V is the volume of the buoy below the ocean wave surface, μ_z is the added mass coefficient of the buoy, and $\hat{\eta}$ is the wave amplitude of the ocean wave. Considering the depth z below the ocean wave surface, the wave amplitude of the ocean wave $\hat{\eta}$ can be written as

$$\hat{\eta} = Ae^{ikz}, \tag{3}$$

where A is the amplitude of the ocean wave surface, i represents the imaginary part of the complex representation, and $k = \omega^2/g$ is the angular wave number of ocean waves. From Equation (3), it can be concluded that a greater depth z below the ocean wave surface leads to a smaller amplitude of the ocean wave.

Moreover, the radiation force $\hat{F}_r$, the hydrostatic buoyancy force $\hat{F}_b$, and the friction force $\hat{F}_f$ can be written as

$$\hat{F}_r = \left(\omega^2 m_z - i\omega R_z\right)\frac{\hat{a}_z}{-\omega^2}, \quad (4)$$

$$\hat{F}_b = -\rho g S_w \frac{\hat{a}_z}{-\omega^2}, \quad (5)$$

$$\hat{F}_f = -i\omega R_f \frac{\hat{a}_z}{-\omega^2}, \quad (6)$$

where m_z and R_z are the added mass and damping coefficient of the buoy, respectively, R_f is the friction resistance coefficient of the double-buoy OWECS.

According to the relationship between speed and acceleration, the vertical direction acceleration $\hat{a}_z$ can be written as

$$\hat{a}_z = i\omega\hat{v}_z, \quad (7)$$

where $\hat{v}_z$ is the vertical direction speed. Substituting Equations (2) and (4)–(7) into (1), the vertical direction speed of buoy can be described as

$$\hat{v}_z = \frac{\left[\rho g S_w - \omega^2 \rho V(1+\mu_z)\right]\hat{\eta}}{i\omega[m+m_z] + \left[R_f + R_z\right] + \frac{\rho g S_w}{i\omega}}. \quad (8)$$

For double-buoy OWECS (see Figure 2b), the basic parameters of double buoys are shown in Table 1. Because the diameters of buoys are smaller than the wavelength of ocean waves, the added mass can be approximately expressed as $m_z = 0.17\rho D^3$, where D is the diameter of buoys, and the damping coefficient R_z can be ignored. It is assumed that the ocean waves are regular; then, according to Equations (3) and (8) and the basic parameters of double buoys, the vertical direction speeds of the outer buoy and inner buoy are illustrated in Figure 3. Figure 3 indicates that a relative motion between the outer buoy and inner buoy occurs, which drives the generator (installed in the upper end of inner buoy) to convert ocean wave energy into electrical energy.

Table 1. The basic parameters of double buoys.

	Outer Diameter	**2.4 m**
Outer buoy	Inner diameter	1.0 m
	Height	1.8 m
	Draft (h_1)	0.771 m
Inner buoy	Outer diameter	0.83 m
	Height	7.9 m
	Draft (h_2)	6.059 m

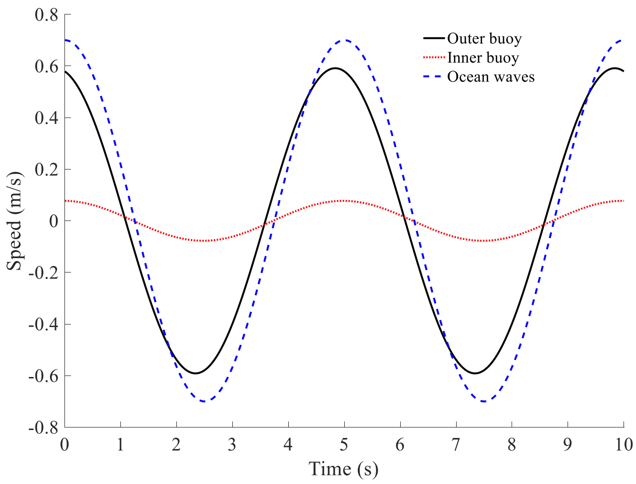

Figure 3. The vertical direction speed of the outer buoy and inner buoy.

2.2. Analysis of Energy Conversion Efficiency

According to the theory of mechanical vibration, only when the resonance condition occurs is the vertical direction displacement of the buoy maximized; thus, the energy conversion efficiency from ocean wave energy into mechanical energy is maximum [18]. For the double-buoy OWECS, the resonance condition means that the outer buoy's vertical direction speed $\hat{v}_z$ is consistent with its vertical direction ocean wave force $\hat{F}_z$ (phase difference is zero), and the inner buoy is nearly stationary. It can be concluded from Equation (8) that the angular frequency ω plays an important role in the phase difference between the vertical direction ocean wave force $\hat{F}_z$ and the vertical direction speed $\hat{v}_z$.

According to Equation (8), Table 1, and certain regular ocean waves with different period T, Figure 4 shows the outer buoy's vertical direction ocean wave force and vertical direction speed, and Table 2 lists the theoretical conversion efficiency from the ocean wave power into the outer buoy and inner buoy's mechanical power. In Table 2, the wave power is calculated as the product of wave surface power J and the buoy's horizontal cross-section S_w, and the wave surface power J can be expressed as

$$J = \frac{\rho g^2}{32\pi} T H^2, \tag{9}$$

where T is the wave period, and H is the wave height. In addition, it should be noted that the ocean wave power consists of kinetic energy (50%) and potential energy (50%), and only the kinetic energy can be converted into the buoy's mechanical power.

Table 2. The theoretical conversion efficiency from ocean wave power into the buoy's power.

Wave Amplitude (m)	Wave Period (s)	Power (kW)			Efficiency
		Ocean Wave (Kinetic Energy)	Outer Buoy	Inner Buoy	
0.7	3	10.7275	3.4206	0.5225	27.02%
0.7	5	17.879	7.0680	0.5615	36.39%
0.7	7	25.0305	6.3139	0.5258	23.12%
0.7	8	28.6065	5.9704	0.5189	19.06%

Table 2 indicates that, for the geometry of the outer buoy of a double-buoy OWECS (see Table 1), there is an optimal ocean wave period which can convert ocean wave energy into the maximum mechanical power of the outer buoy (under the natural operation state), and the optimal ocean wave period T is about 5 s.

The Yellow Sea near Lianyungang port was the installation site of the double-buoy type OWECS; accordingly, the average wave period T and average angular frequency ω in this area are listed in the Table 3 [19]. The average wave period T in the four seasons is about 5 s, which is suitable for the operation of a double-buoy type OWECS. Actually, the real ocean waves are irregular, and the efficiency of the outer buoy should be lower than that of the regular waves. However, the analysis of conversion efficiency based on the regular waves would provide some reference for the design and experimental test of double-buoy ocean wave energy conversion in real ocean waves.

Table 3. The average wave periods and frequencies in Yellow Sea near Lianyungang port.

Season	Average Wave Periods T	Average Angular Frequency ω
Spring	5–5.5 s	1.1424–1.2566 rad/s
Summer	5.5–6 s	1.0472–1.1424 rad/s
Autumn	5–5.5 s	1.1424–1.2566 rad/s
Winter	5–5.5 s	1.1424–1.2566 rad/s

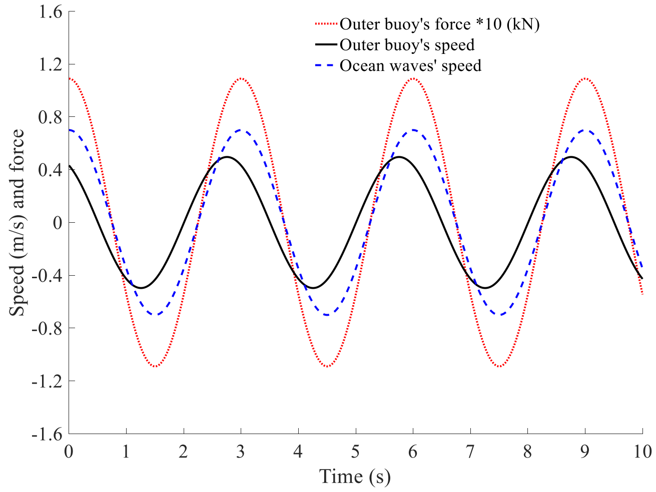

(**a**) Wave period $T = 3s$

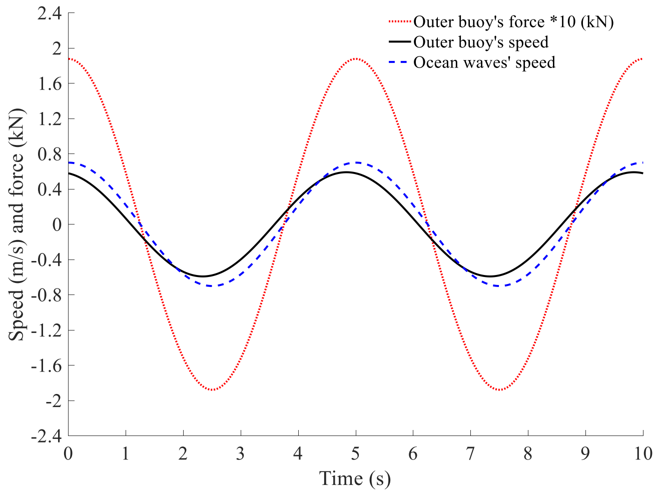

(**b**) Wave period $T = 5s$

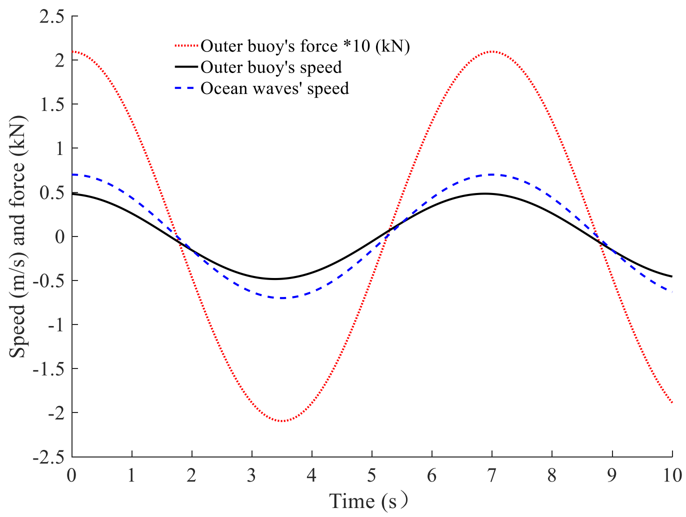

(**c**) Wave period $T = 7s$

Figure 4. The vertical direction force and speed of outer buoy.

3. Experimental Results

According to the efficiency analysis of ocean wave power conversion into the outer buoy's mechanical power, a double-buoy OWECS based on the parameters of Table 1 was constructed and experimented in the Yellow Sea near Lianyungang port. The main components of the double-buoy OWECS included the outer buoy, inner buoy, linear generator, data collector, etc.

3.1. The Specific Structure of Double-Buoy OWECS

Figure 5 shows the overall structure of the linear generator, inner buoy, measuring device, outer buoy, and double-buoy OWECS. In Figure 5a, the linear generator is a permanent magnet tube, which is more suitable for use in an OWECS than a rotary generator. Figure 5b shows the internal structure of inner buoy, in which the linear generator is installed in the upper end of inner buoy. Figure 5c shows the measuring device, including the data collector, data processor, power supply, and data transmission. Figure 5d shows the overall structure of the double-buoy OWECS, with the measuring device installed in the headspace of the outer buoy.

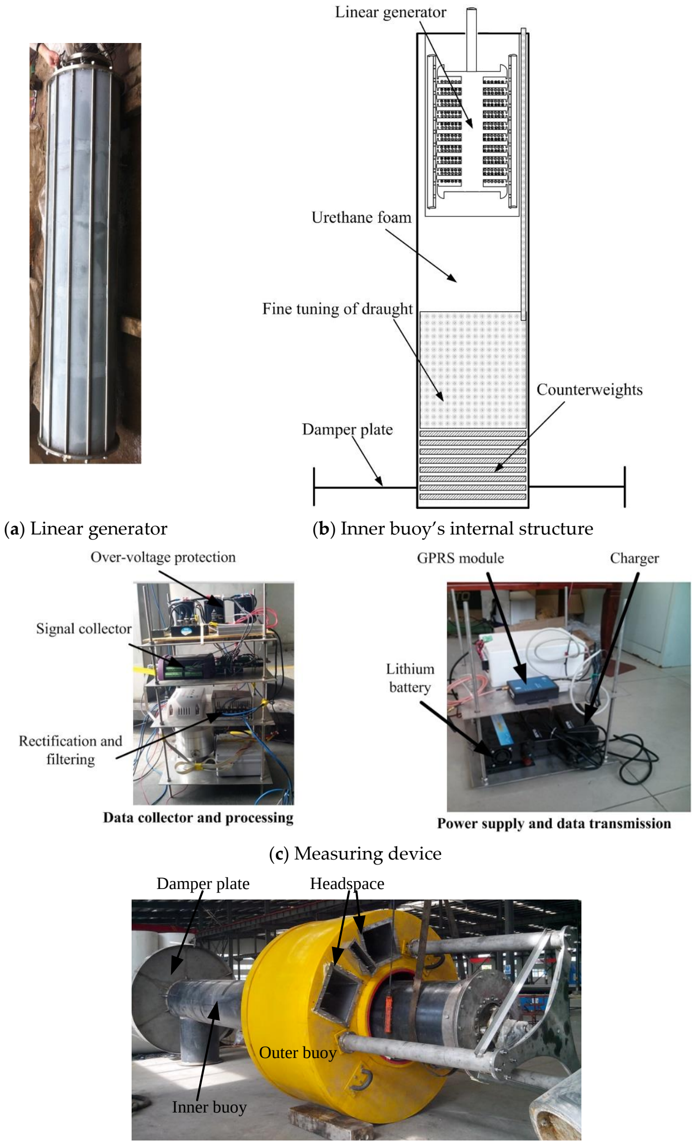

(**a**) Linear generator (**b**) Inner buoy's internal structure

(**c**) Measuring device

(**d**) Total structure

Figure 5. The specific structure of the double-buoy OWECS.

Furthermore, a diagram of the measuring device is shown in Figure 6. As shown in Figure 6, the output voltage of the linear generator (from the double-buoy OWECS) is transformed into 0–5 V by voltage regulation and sampled by the MCU (microcontroller unit). Then, the sampled data can be stored in flash memory or transmitted to the server via a GPRS module. In addition, the function of the relay is overvoltage protection.

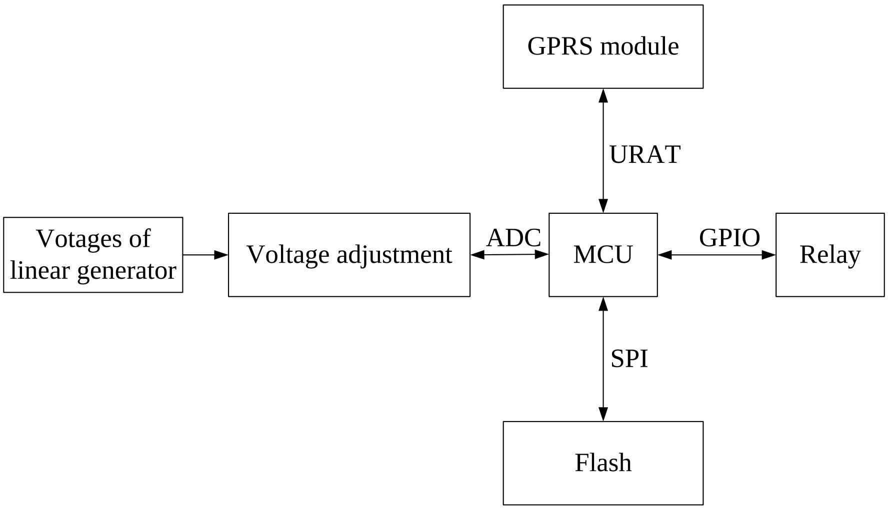

Figure 6. Diagram of measuring device.

3.2. Output Voltage and Power Analysis

Figure 7a shows the installation process of the double-buoy OWECS in the Yellow Sea near Lianyungang port, and Figure 7b shows its operation in ocean waves.

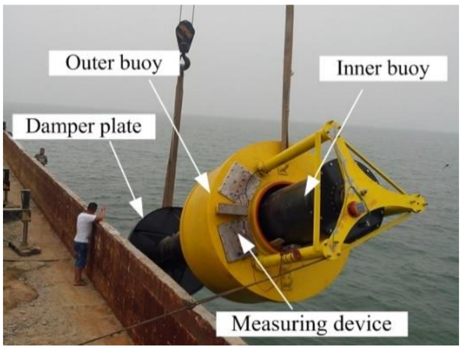

(**a**) Installation process of outer buoy and inner buoy

(**b**) Double-buoy OWECS in ocean waves

Figure 7. The installation process and operation of OWECS.

Figure 8a,b show the output load voltages of the double-buoy OWECS collected by the measuring device. Figure 8c is a power analysis of Figure 8a,b, in which the average power is 1.176 kW, and the maximum power is 4.254 kW.

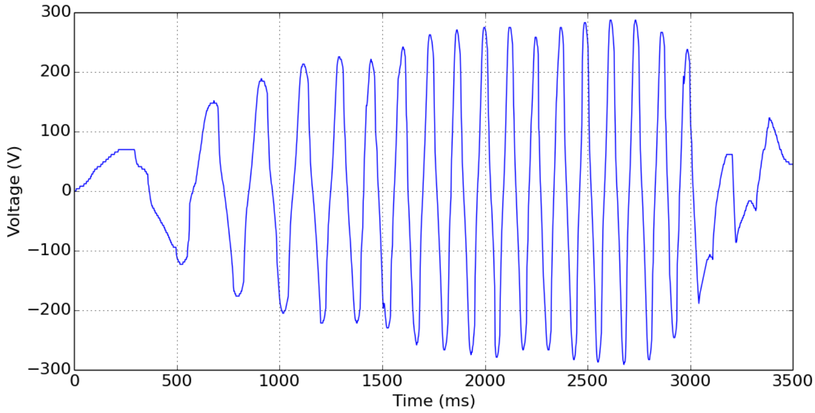

(**a**) Single-phase load voltage

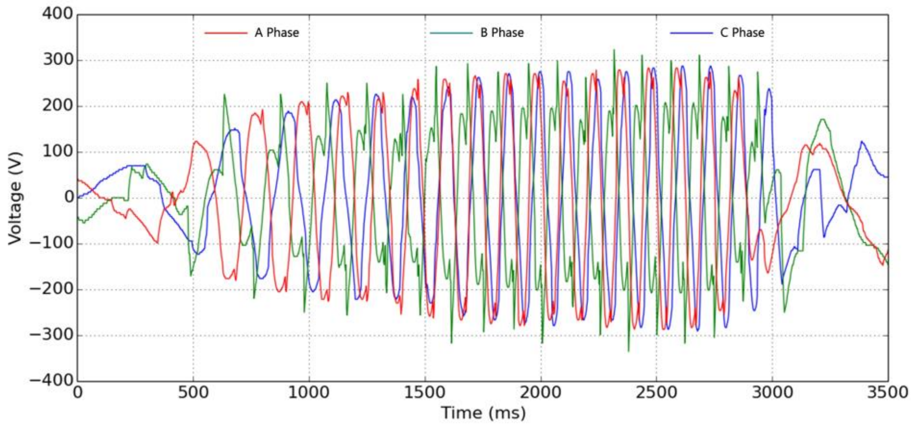

(**b**) Three-phase load voltages

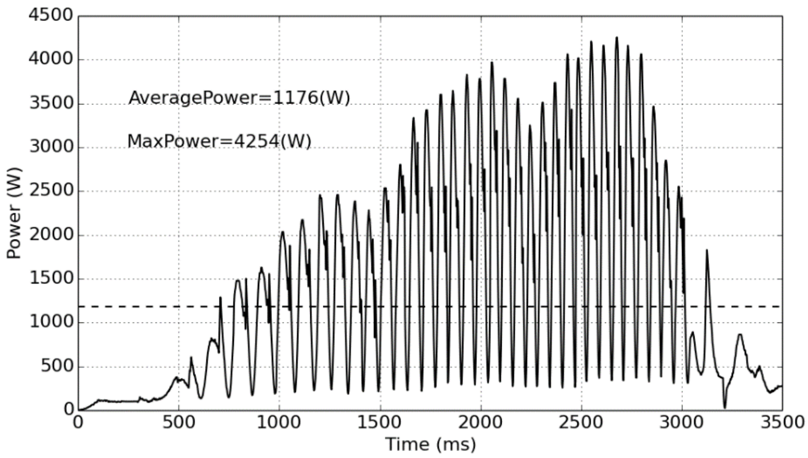

(**c**) Power analysis

Figure 8. Output load voltages and power analysis (the ocean wave period is about 5.5 s).

The output load voltages in Figure 8a,b indicate that the ocean wave period at the same time is about 5.5 s, and the ocean wave amplitude is about 0.7 m (based on the linear generator's voltage–speed characteristic). Under this assumption, according to Equation (9), the experiment conversion efficiency from ocean wave power into electric power is 5.98% (the linear generator's output electric power divided by the ocean wave power).

In addition, if the ocean wave period is longer than 5.5 s, in the case of 8.5 s, the output load voltage of the double-buoy OWECS is as shown in Figure 9a,b, along with the average power (1.187 kW) and maximum power (2.34 kW). Furthermore, according to Equation (9), the experiment conversion efficiency from ocean wave power into electric power is 3.4%.

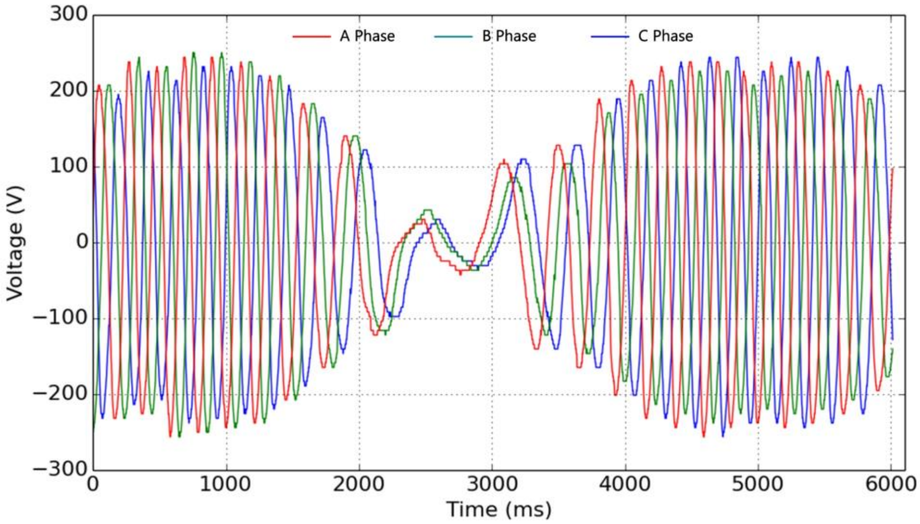

(**a**) Three-phase load voltage

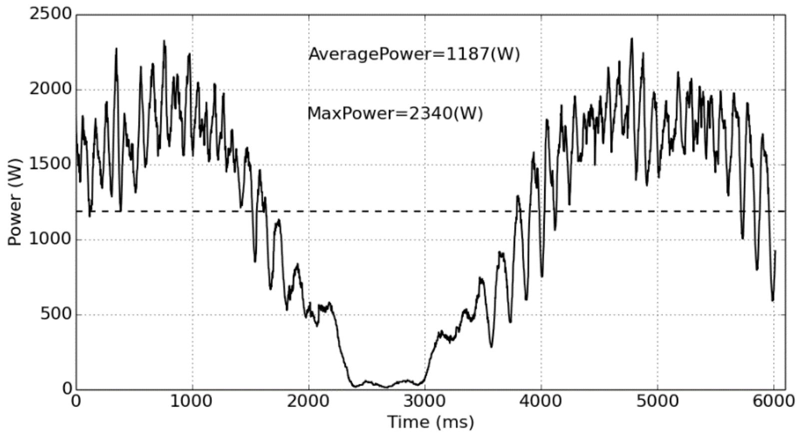

(**b**) Power analysis

Figure 9. Output load voltages and power analysis (the ocean wave period is about 8.5 s).

Table 4 shows the experiment conversion efficiency from ocean wave power into electric power, when the ocean wave periods are 5.5 s and 8.5 s.

Table 4. The experiment conversion efficiency from ocean wave power into electric power.

Wave Amplitude (m)	Wave Period (s)	Power (kW)		Efficiency
		Ocean Wave (Kinetic Energy)	Linear Generator	
0.7	5.5	19.667	1.176	5.98%
0.75	8.5	34.8915	1.187	3.4%

4. Efficiency Improvement of Double-Buoy OWECS

As shown in Table 4, in the natural ocean environment, the operational efficiency of the double-buoy OWECS is low. Furthermore, irregular ocean waves further reduce the operation efficiency. Therefore, considering the operation characteristics of a linear generator, an optimized control method is proposed to increase the operational efficiency of the double-buoy OWECS.

For the double-buoy OWECS, the load force of the linear generator should be considered. Therefore, the vertical direction speed of the floating buoy in the double-buoy OWECS can be written as

$$\hat{v}_z = \frac{\left[\rho g S_w - \omega^2 \rho V (1+\mu_z)\right]\hat{\eta} + \hat{F}_u}{i\omega[m+m_z] + \left[R_f + R_z\right] + \frac{\rho g S_w}{i\omega}}, \tag{10}$$

where $\hat{F}_u$ is the load force of linear generator. For the linear generator, the relationship between load force $\hat{F}_u$ and the q-axis current is described below.

4.1. The Relationship between Load Force and q-Axis Current of Linear Generator

According to the theory of electrical engineering [20], the Park transformation can be written as

$$\begin{bmatrix} s_a \\ s_b \\ s_c \end{bmatrix} = \begin{bmatrix} \cos(\theta) & -\sin(\theta) & 1 \\ \cos(\theta - 120^\circ) & -\sin(\theta - 120^\circ) & 1 \\ \cos(\theta + 120^\circ) & -\sin(\theta + 120^\circ) & 1 \end{bmatrix} \begin{bmatrix} s_d \\ s_q \\ s_0 \end{bmatrix} = Park^{-1} \begin{bmatrix} s_d \\ s_q \\ s_0 \end{bmatrix}, \tag{11}$$

where s_a is the voltage, s_b is the current, and s_c is the magnetic linkage in the form of *abc* coordinates. Moreover, s_d is the voltage, s_q is the current, and s_0 is the magnetic linkage in the form of $dq0$ coordinates.

In the form of *abc* coordinates, the active power output of the linear generator can be written as

$$\hat{P} = \hat{V}_a \hat{i}_a + \hat{V}_b \hat{i}_b + \hat{V}_c \hat{i}_c, \tag{12}$$

where $\hat{V}_a$, $\hat{V}_b$, and $\hat{V}_c$ are the voltages, and $\hat{i}_a$, $\hat{i}_b$, and $\hat{i}_c$ are the currents. Substituting Equation (11) into (12), the active power output of linear generator can be rewritten as

$$\hat{P} = \begin{bmatrix} \hat{V}_a & \hat{V}_b & \hat{V}_c \end{bmatrix} \begin{bmatrix} \hat{i}_a \\ \hat{i}_b \\ \hat{i}_c \end{bmatrix} = Park \begin{bmatrix} \hat{V}_d \\ \hat{V}_q \\ \hat{V}_0 \end{bmatrix}^{-1} \cdot Park^{-1} \begin{bmatrix} \hat{i}_d \\ \hat{i}_q \\ \hat{i}_0 \end{bmatrix} = \frac{3}{2}\left(\hat{V}_d \hat{i}_d + \hat{V}_q \hat{i}_q + 2\hat{V}_0 \hat{i}_0\right), \tag{13}$$

where $\hat{V}_d$, $\hat{V}_q$, and $\hat{V}_0$ are the voltages, and $\hat{i}_d$, $\hat{i}_q$, and $\hat{i}_0$ are the currents. Furthermore, the voltages in $dq0$ coordinates can be described as

$$\begin{cases} \hat{V}_d = R_s \hat{i}_d + L_s \frac{d\hat{i}_d}{dt} - \omega_G L_s \hat{i}_q \\ \hat{V}_q = R_s \hat{i}_q + L_s \frac{d\hat{i}_q}{dt} + \omega_G L_s \hat{i}_d + \omega_G \psi_G \\ \hat{V}_0 = R_s \hat{i}_0 + L_s \frac{d\hat{i}_0}{dt} \end{cases}, \tag{14}$$

where R_s is the resistance, L_s is the inductance, ω_G is the angular frequency, and ψ_G is the magnetic linkage.

In the form of $dq0$ coordinates with a winding delta connection, the zero-sequence voltage H does not exist. Therefore, Equation (13) can be rewritten as

$$\hat{P} = \frac{3}{2}\left(\hat{V}_d \hat{i}_d + \hat{V}_q \hat{i}_q\right). \tag{15}$$

Substituting Equation (14) into (15), the active power output of a linear generator can be rewritten as

$$\hat{P} = \frac{3}{2}\left(R_s\hat{i}_d^2 + R_s\hat{i}_q^2\right) + \frac{3}{2}L_s\left(\hat{i}_d\frac{d\hat{i}_d}{dt} + \hat{i}_q\frac{d\hat{i}_q}{dt}\right) + \frac{3}{2}\omega_G\psi_G\hat{i}_q. \tag{16}$$

On the right side of Equation (16), the first term is copper loss, the second term is the increasing rate of magnetic energy, and the last term is the electromagnetic power.

According to the structure of a linear generator, the relationship between the linear generator's angular frequency ω_G and speed $\hat{v}_z$ is

$$\hat{v}_z = 2f_G\tau = 2\frac{\omega_G}{2\pi}\tau = \frac{\omega_G}{\pi}\tau \Rightarrow \omega_G = \frac{\pi}{\tau}\hat{v}_z, \tag{17}$$

where speed $\hat{v}_z$ is also the relative speed between the outer buoy and inner buoy (see the inner buoy's structure in Figure 5b), τ is the pole pitch, and f_G is the current frequency.

Substituting Equation (17) into the electromagnetic power term of Equation (16), and ignoring the first term (copper loss) and second term (increasing rate of magnetic energy), the electromagnetic power of a linear generator can be described as

$$\hat{P}_{em} = \frac{3}{2}\frac{\pi\psi_G}{\tau}\hat{i}_q\hat{v}_z. \tag{18}$$

For a linear generator, the relationship between electromagnetic power and piston speed is $\hat{P}_{em} = -\hat{F}_u\hat{v}_z$. Thus, the load force $\hat{F}_u$ can be expressed using the q-axis current $\hat{i}_q$ of $dq0$ coordinates.

$$\hat{F}_u = -\frac{3}{2}\frac{\pi\psi_G}{\tau}\hat{i}_q. \tag{19}$$

4.2. Optimized Control of Double-Buoy OWECS

According to the mechanical vibration theory [13], only when the vertical direction motion phase between the outer buoy and ocean waves is identical (in the resonance condition) can the operational efficiency of double buoys type OWECS be improved. Equations (10), (16), and (19) indicate that the vertical direction motion phase between the outer buoy and ocean waves can be synchronized by adjusting the q-axis current $\hat{i}_q$ and d-axis current $\hat{i}_d$. Therefore, on the basis of the q-axis current $\hat{i}_q$ and d-axis current $\hat{i}_d$ of a linear generator, a sliding mode control method is proposed to improve the operational efficiency of a double-buoy OWECS.

Figure 10a shows the detailed control structure of a double-buoy OWECS, including the ocean wave's vertical direction speed $\hat{v}_z^*$, outer buoy's vertical direction speed $\hat{v}_z$, sliding mode control method (SMC), proportional integral (PI) control method, linear generator, Park transformation, power inverter, and space vector pulse width modulation (SVPWM). If the detailed signal transmission process of the voltages and currents in Figure 10a is ignored, the simplified control structure of a double-buoy OWECS is shown in Figure 10b. In Figure 10b, an interference term is added to test the anti-interference ability of the sliding mode control method.

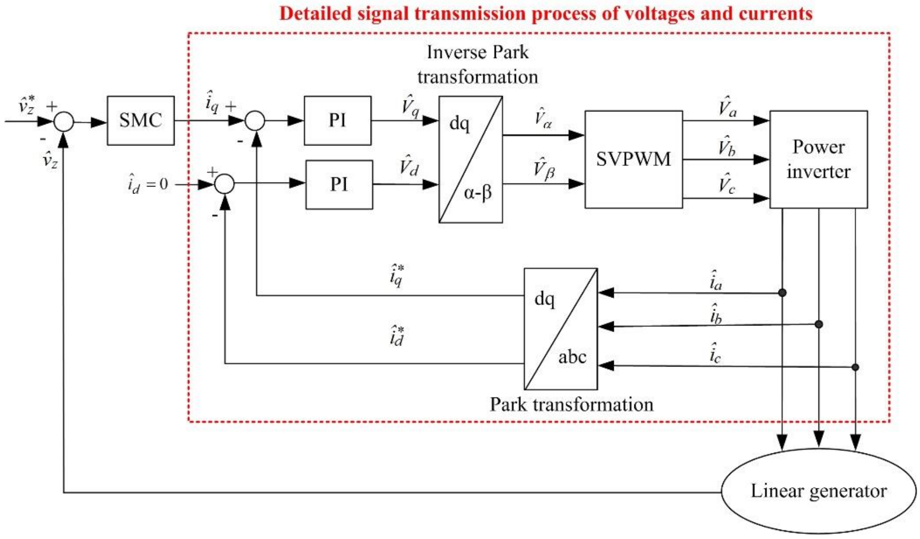

(**a**) Detailed control structure

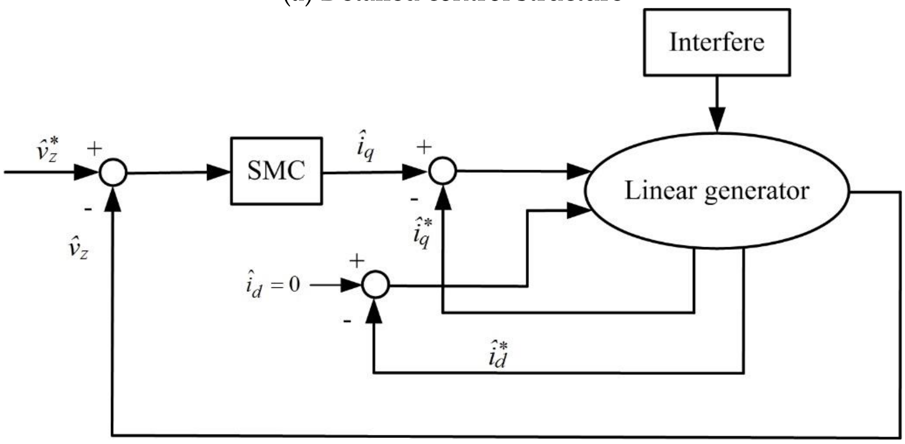

(**b**) Simplified control structure (block diagram)

Figure 10. The control structure of double-buoy OWECS.

According to the principle of mechanical motion [21,22], the motion equation of a linear generator can be written as

$$J\frac{d\omega_m}{dt} = T_L - T_e, \tag{20}$$

$$T_e = \frac{3}{2}P_n i_q \psi_f, \tag{21}$$

where J is the moment of inertia, ω_m is the mechanical angular speed, T_L is the driving torque, T_e is the electromagnetic torque, P_n is the pole-pair number, and ψ_f is the flux linkage.

The method of sliding mode control is adopted [23,24], and the d-axis current is set to $i_d = 0$; then, the expression of q-axis current control can be obtained as

$$i_q^* = \frac{2J}{3P_n\psi_f}\int_0^t \left(c\frac{3}{2J}P_n\psi_f i_q - g\,\mathrm{sgn}(s) - ks\right)dt, \tag{22}$$

where c is the coefficient of the sliding mode surface, k is the constant-velocity approach rate, $\mathrm{sgn}(s)$ is the symbolic function, and g is the exponential approach rate.

Assuming that the moment of inertia of the linear generator is $J = 2$ and the interference term is $d(t) = 10\sin(\omega_g t)$, the simulation optimization control result of the double-buoy OWECS according to the sliding mode control method is shown in Figure 11.

Figure 11a is the simulation control result with a regular ocean wave, while Figure 11b is that with an irregular ocean wave. Figure 11 indicates that the vertical direction motion phase between ocean wave and linear generator (also is the outer buoy) can be synchronized using the appropriate parameter settings of the sliding mode control method; thus, the operational efficiency of a double-buoy OWECS can be improved.

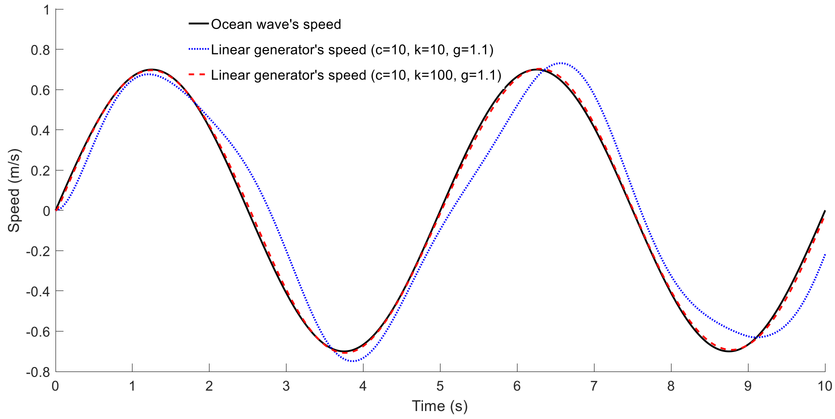

(**a**) In the regular ocean wave

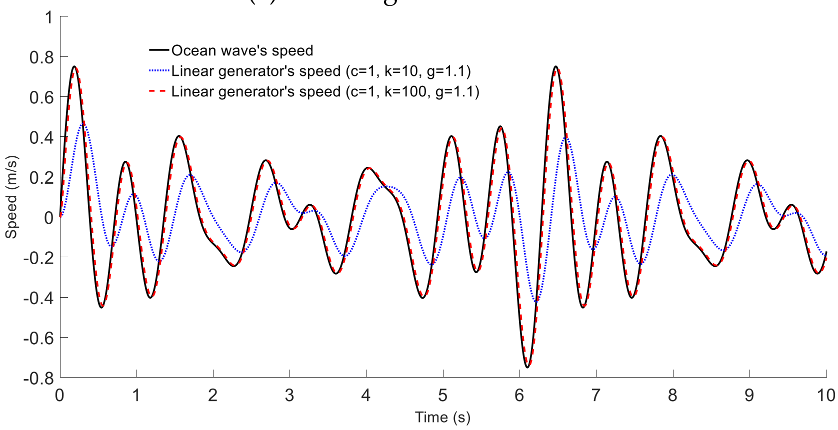

(**b**) In the irregular ocean wave

Figure 11. Optimized control of double-buoy OWECS.

5. Discussion

On the basis of modeling and experimental analysis, an optimized control method was proposed to improve the conversion efficiency of a double-buoy OWECS. However, there are several points should be considered before the practical application of optimized control of double-buoy OWECSs.

Firstly, some details of the optimized control method should be further investigated, such as the signal processing of the linear generator, hardware circuit design, and electronic component selection.

Secondly, the best match between the outer buoy and linear generator should be analyzed. For example, if the maximum output electromagnetic torque of the linear generator is less than the vertical direction ocean wave force of the outer buoy, the optimized control of a double-buoy OWECS will not be realized.

Lastly, due to the existence non-sinusoidal and irregular ocean waves, a small prototype test needs to be implemented before the ocean test, which is beneficial to the improvement and perfection of a double-buoy OWECS. In the process of small prototype tests, the structure size design, parameter setting of control method, anti-interference performance and so on should be tested and improved.

In general, the principal restrictions of study in this paper were the experimental test of the OWECS, the safety of the OWECS in a harsh ocean environment (hurricanes, typhoons, etc.), the efficiency of the SMC method, and the ratio of investment and output, which should be considered and analyzed. For example, after about 3 days of the ocean test (see Figure 7), the OWECS was damaged by the high amplitude of ocean waves during a typhoon. Therefore, from the perspective of scientific research, the safety and high efficiency of the OWECS will be the main research topics in the near future.

6. Conclusions

In this paper, the motion model of a double-buoy OWECS was analyzed, and the correctness of the motion model was verified using an experimental test. However, the analysis of experimental test results indicated that the efficiency of the double-buoy OWECS was lower. Therefore, a sliding mode control method based on a linear generator was proposed to improve the efficiency of the double-buoy OWECS, and some simulation analysis results were presented. After modeling, experimental analysis, and optimized control of the double-buoy OWECS, a discussion was carried out, which may benefit future ocean tests of OWECSs.

Author Contributions: Conceptualization, Z.C. and X.L.; methodology, Z.C.; writing—original draft preparation, Z.C. and Y.C.; writing—review and editing, L.H. All authors have read and agreed to the published version of the manuscript.

Funding: This work was financially supported by the Scientific and Technological Project in Henan Province under Grant No. 222102240037 and No. 222102240106.

Institutional Review Board Statement: Not applicable.

Informed Consent Statement: Not applicable.

Data Availability Statement: Some or all data and models generated or used during the study are available in a repository or online.

Conflicts of Interest: The authors declare no conflict of interest.

References

1. Mustapa, M.A.; Yaakob, O.B.; Ahmed, Y.M.; Rheem, C.K.; Koh, K.K.; Adnan, F.A. Wave energy device and breakwater integration: A review. *Renew. Sustain. Energy Rev.* **2017**, *77*, 43–58. [CrossRef]
2. Brodersen, K.M.; Bywater, E.A.; Lanter, A.M.; Schennum, H.H.; Furia, K.N.; Sheth, M.K.; Kiefer, N.S.; Cafferty, B.K.; Rao, A.K.; Garcia, J.M.; et al. Direct-drive ocean wave-powered batch reverse osmosis. *Desalination* **2022**, *523*, 115393. [CrossRef]
3. Fischer, A.; Silva, J.S.; Beluco, A. Feasibility limits for a hybrid system with ocean wave and ocean current power plants in southern coast of brazil. *Comput. Water Energy Environ. Eng.* **2021**, *10*, 104581. [CrossRef]
4. Viet, N.V.; Wang, Q.; Carpinteri, A. Development of an ocean wave energy harvester with a built-in frequency conversion function. *Int. J. Energy Res.* **2018**, *42*, 684–695. [CrossRef]
5. Edwards, E.C.; Yue, K.P. Optimisation of the geometry of axisymmetric point-absorber wave energy converters. *J. Fluid Mech.* **2022**, *933*, 1–17. [CrossRef]
6. Qin, H.; Tan, S.; Xia, Z.; Zhu, Y. An analysis of international patents on ocean wave energy. *Libr. Inf. Stud.* **2012**, *4*, 45–53.
7. Cheng, Y.; Fu, L.; Dai, S.; Collu, M.; Cui, L.; Yuan, Z.; Incecik, A. Experimental and numerical analysis of a hybrid WEC-breakwater system combining an oscillating water column and an oscillating buoy. *Renew. Sustain. Energy Rev.* **2022**, *169*, 112909. [CrossRef]
8. Cheng, Y.; Fu, L.; Dai, S.; Collu, M.; Ji, C.; Yuan, Z.; Incecik, A. Experimental and numerical investigation of WEC-type floating breakwaters: A single-pontoon oscillating buoy and a dual-pontoon oscillating water column. *Coast. Eng.* **2022**, *177*, 104188. [CrossRef]
9. Jia, C.; Cao, H.; Pan, H.; Ahmed, A.; Jiang, Z.; Azam, A.; Zhang, Z.; Pan, Y. A wave energy converter based on a zero-pressure-angle mechanism for self-powered applications in near-zero energy sea crossing bridges. *Smart Mater. Struct.* **2022**, *31*, 095006. [CrossRef]
10. Baghbani Kordmahale, S.; Do, J.; Chang, K.A.; Kameoka, J. A hybrid structure of piezoelectric fibers and soft materials as a smart floatable open-water wave energy converter. *Micromachines* **2021**, *12*, 1269. [CrossRef] [PubMed]
11. Zou, S.; Abdelkhalik, O. Modeling of a variable-geometry wave energy converter. *IEEE J. Ocean. Eng.* **2021**, *46*, 879–890. [CrossRef]
12. Park, J.S.; Gu, B.G.; Kim, J.R.; Cho, I.H.; Jeong, I.; Lee, J. Active phase control for maximum power point tracking of linear wave generator. *IEEE Trans. Power Electron.* **2017**, *32*, 7651–7662. [CrossRef]
13. Falnes, J. *Ocean Waves and Oscillating Systems*; Cambridge University Press: Cambridge, MA, USA, 2002.
14. Farrok, O.; Islam, M.R.; Sheikh, M.R.; Guo, Y.; Zhu, J.; Xu, W. A novel superconducting magnet excited linear generator for wave energy conversion system. *IEEE Trans. Appl. Supercond.* **2016**, *26*, 1–5. [CrossRef]

15. García-Tabarés, L.; Lafoz, M.; Blanco, M.; Torres, J.; Obradors, D.; Nájera, J.; Navarro, G.; García, F.; Sánchez, A. New type of linear switched reluctance generator for wave energy applications. *IEEE Trans. Appl. Supercond.* **2020**, *30*, 19642959.
16. Xia, T.; Yu, H.; Guo, R.; Liu, X. Research on the field-modulated tubular linear generator with quasi-halbach magnetization for ocean wave energy conversion. *IEEE Trans. Appl. Supercond.* **2018**, *28*, 17610493. [CrossRef]
17. Viet, N.V.; Xie, X.D.; Liew, K.M.; Banthia, N.; Wang, Q. Energy harvesting from ocean waves by a floating energy harvester. *Energy* **2016**, *112*, 1219–1226. [CrossRef]
18. Masoumi, M.; Wang, Y. Repulsive magnetic levitation-based ocean wave energy harvester with variable resonance: Modeling, simulation and experiment. *J. Sound Vib.* **2016**, *381*, 192–205. [CrossRef]
19. Xie, D.M.; Chen, Y.P.; Zhang, C.K. On wave distribution of the East China Sea. *Port Waterw. Eng.* **2012**, *11*, 14–21.
20. Masamichi, I.; Shinji, D. PMSM Model Discretization in Consideration of Park Transformation for Current Control System. In Proceedings of the International Power Electronics Conference, Niigata, Japan, 20–24 May 2018.
21. Liu, K.; Hou, C.; Hua, W. A Novel Inertia Identification Method and Its Application in PI Controllers of PMSM Drives. *IEEE Access* **2016**, *7*, 13445–13454. [CrossRef]
22. Wang, P.; Xu, Y.; Ding, R.; Liu, W.; Shu, S.; Yang, X. Multi-Kernel Neural Network Sliding Mode Control for Permanent Magnet Linear Synchronous Motors. *IEEE Access* **2021**, *9*, 57385–57392. [CrossRef]
23. Liu, J. *Sliding Mode Control Design and MATLAB Simulation: The Basic Theory and design Method*; Tsinghua University Press: Beijing, China, 2015.
24. Wei, Y.; Sun, L.; Chen, Z. An improved sliding mode control method to increase the speed stability of permanent magnet synchronous motors. *Energies* **2022**, *15*, 15176313. [CrossRef]